

Contents lists available at [ScienceDirect](http://ScienceDirect.com)

Physics Letters B

www.elsevier.com/locate/physletb

Observation of the $\Xi_b^- \rightarrow J/\psi \Lambda K^-$ decay



The LHCb Collaboration

ARTICLE INFO

Article history:

Received 19 January 2017

Received in revised form 8 May 2017

Accepted 11 June 2017

Available online 26 June 2017

Editor: M. Doser

ABSTRACT

The observation of the decay $\Xi_b^- \rightarrow J/\psi \Lambda K^-$ is reported, using a data sample corresponding to an integrated luminosity of 3 fb^{-1} , collected by the LHCb detector in pp collisions at centre-of-mass energies of 7 and 8 TeV. The production rate of Ξ_b^- baryons detected in the decay $\Xi_b^- \rightarrow J/\psi \Lambda K^-$ is measured relative to that of Λ_b^0 baryons using the decay $\Lambda_b^0 \rightarrow J/\psi \Lambda$. Integrated over the b -baryon transverse momentum $p_T < 25 \text{ GeV}/c$ and rapidity $2.0 < y < 4.5$, the measured ratio is

$$\frac{f_{\Xi_b^-} \mathcal{B}(\Xi_b^- \rightarrow J/\psi \Lambda K^-)}{f_{\Lambda_b^0} \mathcal{B}(\Lambda_b^0 \rightarrow J/\psi \Lambda)} = (4.19 \pm 0.29 \text{ (stat)} \pm 0.15 \text{ (syst)}) \times 10^{-2},$$

where $f_{\Xi_b^-}$ and $f_{\Lambda_b^0}$ are the fragmentation fractions of $b \rightarrow \Xi_b^-$ and $b \rightarrow \Lambda_b^0$ transitions, and \mathcal{B} represents the branching fraction of the corresponding b -baryon decay. The mass difference between Ξ_b^- and Λ_b^0 baryons is measured to be

$$M(\Xi_b^-) - M(\Lambda_b^0) = 177.08 \pm 0.47 \text{ (stat)} \pm 0.16 \text{ (syst)} \text{ MeV}/c^2.$$

© 2017 The Author(s). Published by Elsevier B.V. This is an open access article under the CC BY license (<http://creativecommons.org/licenses/by/4.0/>). Funded by SCOAP³.

1. Introduction

Since the birth of the quark model, the possibility of forming baryonic states from combinations of quarks other than three valence quarks has been considered [1,2]. For example, states with four quarks and an antiquark, referred to as pentaquarks [3], have been searched for experimentally for many years. As observed with the LHCb detector at the LHC, the distribution of invariant mass of the $J/\psi p$ system in $\Lambda_b^0 \rightarrow J/\psi (\rightarrow \mu^+ \mu^-) p K^-$ decays shows a narrow peak suggestive of $uudc\bar{c}$ pentaquark formation [4–6]. (The inclusion of charge conjugate processes is implied throughout the text.) From a six-dimensional amplitude model fit, two pentaquark resonances, decaying into $J/\psi p$, are observed with large significances [4].

As suggested in Ref. [7], a hidden-charm pentaquark with open strangeness ($udsc\bar{c}$) [8] could be observed as a $J/\psi \Lambda$ state in the decay $\Xi_b^- \rightarrow J/\psi \Lambda K^-$. The decay is similar to $\Lambda_b^0 \rightarrow J/\psi p K^-$, and differs from the latter by exchanging one u spectator quark with an s spectator quark, as illustrated in Fig. 1 (a). An additional diagram can contribute to the Ξ_b^- decay, as illustrated in Fig. 1 (b), where the s spectator quark forms the K^- meson instead of the Λ baryon.

In this Letter, we present the first observation of the $\Xi_b^- \rightarrow J/\psi \Lambda K^-$ decay. Using the decay $\Lambda_b^0 \rightarrow J/\psi \Lambda$ as normalisation

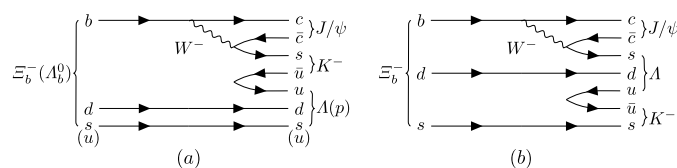


Fig. 1. Feynman diagrams Ξ_b^- and Λ_b^0 decays. Diagram (a) contributes to both $\Lambda_b^0 \rightarrow J/\psi p K^-$ decays and $\Xi_b^- \rightarrow J/\psi \Lambda K^-$ decays, diagram (b) contributes only to the Ξ_b^- decay.

channel, the production rate of the observed Ξ_b^- decays relative to that of Λ_b^0 baryons is measured as

$$R_{\Xi_b^-/\Lambda_b^0} \equiv \frac{f_{\Xi_b^-} \mathcal{B}(\Xi_b^- \rightarrow J/\psi \Lambda K^-)}{f_{\Lambda_b^0} \mathcal{B}(\Lambda_b^0 \rightarrow J/\psi \Lambda)} = \frac{N(\Xi_b^- \rightarrow J/\psi \Lambda K^-)}{N(\Lambda_b^0 \rightarrow J/\psi \Lambda)} \epsilon_{\text{rel}}, \quad (1)$$

where $f_{\Xi_b^-}$ and $f_{\Lambda_b^0}$ are the $b \rightarrow \Xi_b^-$ and $b \rightarrow \Lambda_b^0$ fragmentation fractions, \mathcal{B} represents the branching fraction of the corresponding b -baryon decay, $N(\Xi_b^- \rightarrow J/\psi \Lambda K^-)$ and $N(\Lambda_b^0 \rightarrow J/\psi \Lambda)$ are the signal yields, and $\epsilon_{\text{rel}} = \epsilon(\Lambda_b^0 \rightarrow J/\psi \Lambda)/\epsilon(\Xi_b^- \rightarrow J/\psi \Lambda K^-)$ is their relative efficiency. We also present a measurement of the mass difference between the Ξ_b^- and Λ_b^0 baryons. Measurements

of the Ξ_b^- mass to date have been obtained using absolute mass measurements and a single measurement of the mass difference $\delta M \equiv M(\Xi_b^-) - M(\Lambda_b^0)$ [9]. Earlier measurements from the Tevatron [10] are, however, in tension (2.1 standard deviations) with the recent and most precise value from the LHCb experiment [11], obtained from the measurement of δM . The present analysis offers an opportunity to provide a second precise measurement of δM using a data sample that is statistically independent of other measurements of the Ξ_b^- mass from LHCb.

2. Data sample and detector

The measurement is based on a data sample corresponding to 1 fb^{-1} of integrated luminosity collected by the LHCb experiment in pp collisions at 7 TeV centre-of-mass energy in 2011, and 2 fb^{-1} at 8 TeV in 2012. The LHCb detector [12,13] is a single-arm forward spectrometer covering the pseudorapidity range $2 < \eta < 5$, designed for the study of particles containing b or c quarks. The detector includes a high-precision tracking system consisting of a silicon-strip vertex detector (VELO) surrounding the pp interaction region, a large-area silicon-strip detector located upstream of a dipole magnet with a bending power of about 4 Tm, and three stations of silicon-strip detectors and straw drift tubes placed downstream of the magnet. The tracking system provides a measurement of momentum, p , of charged particles with a relative uncertainty that varies from 0.5% at low momentum to 1.0% at 200 GeV/c. The minimum distance of a track to a primary vertex (PV), the impact parameter (IP), is measured with a resolution of $(15 + 29/p_T) \mu\text{m}$, where p_T is the component of the momentum transverse to the beam, in GeV/c. Different types of charged hadrons are distinguished using information from two ring-imaging Cherenkov (RICH) detectors. Photons, electrons and hadrons are identified by a calorimeter system consisting of scintillating-pad and preshower detectors, an electromagnetic calorimeter and a hadronic calorimeter. Muons are identified by a system composed of alternating layers of iron and multiwire proportional chambers.

The online event selection is performed by a trigger [14], which consists of a hardware stage, based on information from the calorimeter and muon systems, followed by a software stage. For this analysis, triggers that select J/ψ candidates are used for both signal and normalisation channels. The hardware trigger requires at least one muon with $p_T > 1.48$ (1.76) GeV/c, or two muons with $\sqrt{p_T(\mu_1)p_T(\mu_2)} > 1.3$ (1.6) GeV/c, in the 2011 (2012) data sample. The subsequent software trigger is composed of two stages, the first of which performs a partial reconstruction and requires either a pair of well-reconstructed, oppositely charged muons having an invariant mass above $2.7 \text{ GeV}/c^2$, or a single well-reconstructed muon with $p_T > 1 \text{ GeV}/c$ and high IP at all PVs of the event. The second stage of the software trigger requires a pair of oppositely charged muons to form a good-quality vertex that is well separated from all PVs, and which has an invariant mass within $\pm 120 \text{ MeV}/c^2$ of the known J/ψ mass [9].

In the simulation, pp collisions are generated using PYTHIA 8 [15,16] with a specific LHCb configuration [17]. Decays of hadronic particles are described by EVTGEN [18], in which final-state radiation is generated using PHOTOS [19]. The interaction of the generated particles with the detector, and its response, are implemented using the GEANT4 toolkit [20,21] as described in Ref. [22]. The signal decays of Λ_b^0 and Ξ_b^- baryons are simulated according to a phase-space model.

3. Selection requirements

The $\Xi_b^- \rightarrow J/\psi \Lambda K^-$ and $\Lambda_b^0 \rightarrow J/\psi \Lambda$ candidates are reconstructed using the decays $J/\psi \rightarrow \mu^+ \mu^-$ and $\Lambda \rightarrow p \pi^-$. An offline selection is applied after the trigger, based on a loose preselection, followed by a multivariate classifier based on a Gradient Boosted Decision Tree (BDTG) [23].

In the preselection, the J/ψ candidates are formed from two oppositely charged particles with $p_T > 500 \text{ MeV}/c$, identified as muons and consistent with originating from a common vertex but inconsistent with originating from any PV. The invariant mass of the $\mu^+ \mu^-$ pair is required to be within $[-48, +43] \text{ MeV}/c^2$ of the known J/ψ mass [9].

The Λ candidates are formed by combining candidate p and π^- particles with large χ_{IP}^2 , where χ_{IP}^2 is defined as the difference in the χ^2 of the vertex fit for a given PV reconstructed with and without the considered particle. Given the long lifetime of the Λ baryon, its decay vertex can be reconstructed either from a pair of tracks that include segments in the VELO, called *long* tracks (LL Λ candidates), or from a pair of tracks reconstructed using only the tracking stations downstream of the VELO, called *downstream* tracks (DD Λ candidates). The invariant mass of the $p \pi^-$ pair is required to be within 4 (6) MeV/c^2 of the known Λ mass [9] for the LL (DD) Λ candidates. For the LL Λ candidates, both the proton and the pion must have $p_T > 250 \text{ MeV}/c$, and pass loose particle identification (PID) criteria based on information provided by the RICH detectors. For the DD Λ candidates, the decay vertex must not be reconstructed in the first half of the VELO. To remove background from $K_S^0 \rightarrow \pi^+ \pi^-$ decays, the reconstructed mass for the LL (DD) Λ candidate under the $\pi^+ \pi^-$ hypothesis is required to be more than 4 (10) MeV/c^2 away from the known K_S^0 mass [9].

The Ξ_b^- and Λ_b^0 candidates are formed from a J/ψ and a Λ candidate, combined with a kaon candidate for the Ξ_b^- baryon, where the kaon candidate must have $p_T > 250 \text{ MeV}/c$ and large χ_{IP}^2 . Each reconstructed b -baryon candidate is required to have $\chi_{\text{IP}}^2 < 25$ with respect to at least one PV, and is associated to the one which the χ_{IP}^2 is smallest. The candidate decay vertex must also have a fit with good χ^2 and a separation of at least 1.5 mm from the PV. The angle, θ , between the b -baryon momentum and the vector from the associated PV to the decay vertex must satisfy $\cos \theta > 0.999$. For both b baryons fiducial cuts of $p_T < 25 \text{ GeV}/c$ and rapidity in the range $2.0 < y < 4.5$ are required to have a well-defined kinematic region in which the measurement is performed. There are only 0.2% events outside the fiducial kinematic region. A kinematic fit [24] is applied to the Ξ_b^- and Λ_b^0 candidates, with the J/ψ and Λ masses constrained to the known values [9], and the b -baryon candidate constrained to point back to its PV. As a result, the mass resolution is improved by 60%, with most of the improvement coming from the constraints on the J/ψ and Λ masses.

The $\Xi_b^- \rightarrow J/\psi \Lambda K^-$ and $\Lambda_b^0 \rightarrow J/\psi \Lambda$ candidates passing the preselection are filtered with a BDTG to further suppress the combinatorial background. For the Ξ_b^- decay, the following discriminating variables are used: the minimum $\text{DLL}_{\mu\pi}$ (defined as the difference in the logarithms of the likelihood values from the particle identification systems [25] for the muon and pion hypotheses) and the minimum p_T within the muon pair; the χ_{IP}^2 of all other final-state tracks and the Λ baryon; the p_T of the p , π , K and J/ψ candidates; the decay length and the vertex fit χ^2 of the Λ candidate; the χ^2 of the kinematic fit, $\cos \theta$ and the decay time of the Ξ_b^- baryon. The BDTG is trained on a simulated $\Xi_b^- \rightarrow J/\psi \Lambda K^-$ sample for the signal; data candidates with $5944 < m(J/\psi \Lambda K) < 6094 \text{ MeV}/c^2$ are used to model the background. The LL and DD samples are trained separately. The optimal

working point on the BDTG response and the PID variable of the kaon is determined by maximising the significance of the expected \mathcal{E}_b^- signal, $S/\sqrt{S+B}$, where S (B) is the expected signal (background) yield in a range corresponding to ± 2.5 times the mass resolution at the known \mathcal{E}_b^- mass [9]. The S value is calculated as the product of an initial signal yield determined from the data at $\text{BDTG} > 0$, and the relative efficiency with respect to the BDTG selection obtained from the simulation. The value of B is estimated from the data sidebands. The final BDTG working point has a signal efficiency of 90% (70%) and a background rejection rate of 97% (99%) for LL (DD) samples.

The normalisation channel uses a separate training for the BDTG, where the variables for the K^- meson are excluded. The background training sample is taken from the $J/\psi \Lambda$ invariant mass regions with $150 < |m(J/\psi \Lambda) - m_{\Lambda_b^0}| < 350 \text{ MeV}/c^2$, where $m_{\Lambda_b^0}$ is the known Λ_b^0 mass [9]. The optimal requirement on the BDTG response for the normalisation mode is the same as for the signal channel. For both samples, in 0.3% of the cases multiple candidates are found, all of which are retained in the analysis.

4. Signal yields

In each of the two categories (LL and DD), a simultaneous extended unbinned maximum likelihood fit to the \mathcal{E}_b^- and Λ_b^0 candidates' invariant mass distributions is performed to determine the respective \mathcal{E}_b^- and Λ_b^0 signal yields. The data, separated by category, and the results of the two fits are shown in Fig. 2.

In the fit of each sample, the signal shape is modelled by a Hypatia function [26]. The mean values and the resolutions of the functions are allowed to vary in the fit, with the ratio of the \mathcal{E}_b^- to Λ_b^0 mass resolution and the tail parameters fixed to the values obtained from simulation. The combinatorial background is modelled by an exponential function whose parameters are determined by the fit. A partially reconstructed background component, which comes from the decay $\mathcal{E}_b^- \rightarrow J/\psi \Sigma^0 K^-$ with $\Sigma^0 \rightarrow \Lambda \gamma$, is taken into account in the $\mathcal{E}_b^- \rightarrow J/\psi \Lambda K^-$ sample. The shape of this background is determined from simulation, and its yield is free to vary in the fit. In each Λ category, the fit is simultaneously done for the signal and control channels. The fit procedure is validated by large sets of pseudo-experiments.

In the LL samples, the signal yields are found to be $N(\mathcal{E}_b^- \rightarrow J/\psi \Lambda K^-) = 99 \pm 12$ and $N(\Lambda_b^0 \rightarrow J/\psi \Lambda) = 4838 \pm 72$. The corresponding values in the DD samples are 209 ± 17 and 12499 ± 125 , respectively. The $\mathcal{E}_b^- \rightarrow J/\psi \Sigma^0 K^-$ background yields are 72 ± 25 and 221 ± 37 in the LL and DD samples, respectively. A likelihood-ratio test $\Delta(2 \ln \mathcal{L}) \equiv -2 \ln(\mathcal{L}_B/\mathcal{L}_{S+B})$ is used to estimate the $\mathcal{E}_b^- \rightarrow J/\psi \Lambda K^-$ signal significance, where \mathcal{L}_B and \mathcal{L}_{S+B} stand for the likelihood values of the background-only hypothesis and the signal plus background hypothesis, respectively. A fit to the combined data samples of LL and DD categories is performed to estimate the total signal significance. The value of $\Delta(2 \ln \mathcal{L})$ is 464.8. Accounting for two additional parameters associated with the signal component in the \mathcal{L}_{S+B} fit, this corresponds to a significance of 21 standard deviations [27].

5. Efficiency corrections

The total efficiency of each decay mode consists of the geometrical acceptance of the detector, the efficiencies of the trigger, the reconstruction and selection, and the hadron identification. The first three efficiency factors are determined from samples of simulated events generated within the kinematic region $p_T < 25 \text{ GeV}/c$ and $2.0 < y < 4.5$ for both b baryons. The hadron PID efficiency is determined using calibration data of $D^{*+} \rightarrow D^0(\rightarrow K^- \pi^+) \pi^+$

Table 1
Relative systematic uncertainty for the ratio $R_{\mathcal{E}_b^-/\Lambda_b^0}$.

Source	Uncertainty (%)
Signal model	0.7
Background model	1.6
BDTG efficiency	0.1
PID efficiency	1.0
Tracking efficiency	1.2
Phase space	1.5
b -baryon kinematics	1.5
\mathcal{E}_b^- and Λ_b^0 lifetime	1.1
Simulation sample size	0.7
Fixed resolution ratio	0.6
Total	3.5

and $\Lambda_c^+ \rightarrow p K^- \pi^+$ decays. Events in the calibration samples are weighted to reproduce the momentum, pseudorapidity and event multiplicity distributions of the hadrons from $\mathcal{E}_b^- \rightarrow J/\psi \Lambda K^-$ and $\Lambda_b^0 \rightarrow J/\psi \Lambda$ decays. The relative efficiency is estimated to be $\epsilon_{\text{rel}} = \epsilon(\Lambda_b^0 \rightarrow J/\psi \Lambda) / \epsilon(\mathcal{E}_b^- \rightarrow J/\psi \Lambda K^-) = 1.964 \pm 0.028$ and 2.191 ± 0.017 for the LL and DD samples, respectively, where the uncertainties are statistical only.

Two correction factors are considered for the relative efficiency to account for differences between data and simulation. The LL and DD samples are combined to derive these factors. The first factor accounts for possible local structures in the data distribution due to intermediate states or nonresonant amplitudes that are generally present in multibody decays. An average efficiency is calculated over the two-dimensional phase space of the $\mathcal{E}_b^- \rightarrow J/\psi \Lambda K^-$ three-body decay,

$$\langle \epsilon \rangle = \sum_i w_i / \sum_i (w_i / \epsilon_{\text{PH}i}), \quad (2)$$

where ϵ_{PH} is the efficiency as a function of the phase-space position obtained from simulation, the numerator represents the number of reconstructed signal candidates, and the denominator represents the efficiency-corrected number of signal candidates; in both cases the sum extends over all \mathcal{E}_b^- candidates in data. The event-by-event signal weight (w_i), is obtained using the *sPlot* technique [28] to subtract the background contribution. The average efficiency is 98% relative to the efficiency obtained using the phase-space simulation.

The second factor accounts for possible differences in p_T and rapidity spectra in b -baryon production in data and simulation. The simulated samples are reweighted in bins of p_T and rapidity, in order to reproduce the data distribution of Λ_b^0 decays, and the relative efficiency is recalculated. The correction factor of this source is 1.138. The value is consistent if separately correcting for the LL and DD samples. The product of the two correction factors for the average efficiency is 1.115. The uncertainties in the correction factors are taken as systematic uncertainties discussed below.

6. Results of $R_{\mathcal{E}_b^-/\Lambda_b^0}$ and systematic uncertainties

Using the yields and efficiencies with corrections, the ratios of $R_{\mathcal{E}_b^-/\Lambda_b^0}$ for the LL and DD data sets are measured to be $(4.46 \pm 0.55) \times 10^{-2}$ and $(4.08 \pm 0.34) \times 10^{-2}$, respectively, where the uncertainties are statistical only. The two independent measurements are consistent with each other. Their weighted average yields $R_{\mathcal{E}_b^-/\Lambda_b^0} = (4.19 \pm 0.29 \pm 0.15) \times 10^{-2}$. Whenever two uncertainties are quoted, the first is statistical and the second is systematic.

The sources of systematic uncertainties for the ratio $R_{\mathcal{E}_b^-/\Lambda_b^0}$ are summarised in Table 1. The quoted values are averages over the LL

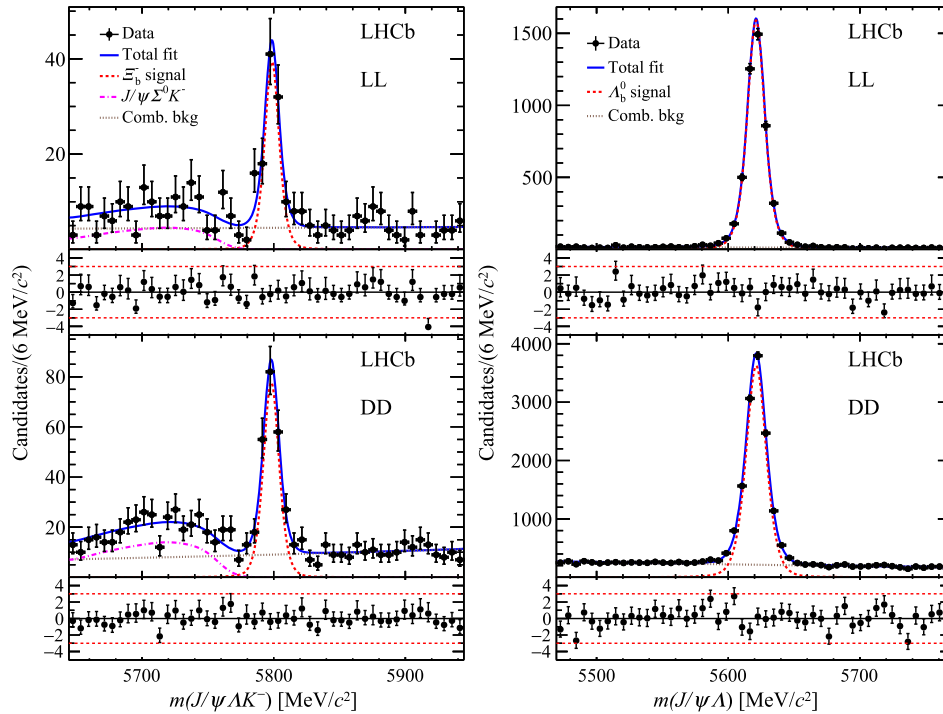


Fig. 2. Reconstructed (left) $\Xi_b^- \rightarrow J/\psi \Lambda K^-$ and (right) $\Lambda_b^0 \rightarrow J/\psi \Lambda$ candidates using (top) LL and (bottom) DD Λ types. The solid (blue) lines show the full fit functions, the dashed (red) lines the signal components, the dot-dashed (purple) lines the $\Xi_b^- \rightarrow J/\psi \Sigma^0 K^-$ background and the dotted (black) lines the combinatorial background. At the bottom of each figure the differences between the data and the fit divided by the uncertainty in the data are shown.

and DD categories. The uncertainty on the relative yields is evaluated by using alternative functions to model each of the fit components. These include changing the signal model from the Hypatia function to a double-sided Crystal Ball function [29], changing the combinatorial background model from the exponential function to a second-order polynomial, and varying the parametrisation of the $\Xi_b^- \rightarrow J/\psi \Sigma^0 K^-$ background. The effect of the latter is found to be negligible. To reduce the statistical fluctuations in the estimate of the systematic uncertainties, large numbers of pseudoexperiments are performed. The parameters of the alternative model are used to generate experiments, which are then fitted by both the alternative and the default models. A Gaussian function is fitted to the distribution of the $R_{\Xi_b^-/\Lambda_b^0}$ difference for these pseudoexperiments and the mean value is assigned as a systematic uncertainty.

There are several sources of systematic uncertainty related to the evaluation of the relative efficiency. Most of them cancel in the ratio of efficiencies, except those related to the additional kaon in the Ξ_b^- decay. The BDTG input variables for background-subtracted $\Lambda_b^0 \rightarrow J/\psi \Lambda$ data are compared to the corresponding simulated distributions, and all of the variables, except for the vertex-fit χ^2 and χ_{IP}^2 for Λ candidates in the DD category, are well modelled. The simulation is then smeared for these two variables to match the data, and the small change of 0.1% in the relative efficiency is taken as systematic uncertainty. The uncertainty due to the kaon PID efficiency is studied by changing the binning scheme in momentum, pseudorapidity and event multiplicity. The alternative binning gives a 1.0% difference in the signal efficiency, which is assigned as a systematic uncertainty. The tracking efficiency is estimated from simulation and calibrated with the data [30]; an uncertainty of 0.4% is assigned for the kaon track. An additional systematic uncertainty of 1.1% is assigned to the kaon tracking efficiency due to an imperfect knowledge of the material budget in the detector [5]. It is estimated from simulation by changing the used interaction length in the detector by 10%. The total tracking-

efficiency related systematic uncertainty, adding the two contributions in quadrature, is 1.2%.

The systematic uncertainty of the average efficiency defined in Eq. (2) is 1.5%, calculated by propagating the statistical uncertainties for the efficiencies over the phase space. In reweighting the simulated p_T and y spectra to match the data, an uncertainty of 1.5% is estimated by varying the weights for each kinematic bin by its uncertainty. The uncertainties in the Λ_b^0 lifetime of 1.468 ± 0.012 ps [31] and the Ξ_b^- lifetime of 1.57 ± 0.04 ps [9], result in relative changes of $\pm 0.2\%$ and $\pm 1.1\%$ in the efficiencies, respectively. The limited size of the simulated samples gives rise to an uncertainty of 0.7%. Varying the mass resolution ratios of the Ξ_b^- to Λ_b^0 mass peaks, which are fixed in the nominal fit to the data, results in an uncertainty of 0.6%. The uncertainty due to the trigger efficiency is cancelled between the signal and control modes, as the trigger requirements are imposed only on the muon pairs. Finally, the total relative systematic uncertainty is 3.5%, obtained by adding all of the above contributions in quadrature.

7. Measurement of the mass difference

The mass difference, δM , is obtained from a single simultaneous fit to four mass distributions, consisting of the LL and DD samples for both the Ξ_b^- and Λ_b^0 candidates. The ratio $R_{\Xi_b^-/\Lambda_b^0}$ is also a freely varying parameter in this second fit for δM . Compared to the fits described in the previous section, the new fit has two less free parameters: for each of the Λ categories, δM is constrained to be the same value and $N(\Xi_b^- \rightarrow J/\psi \Lambda K^-)$ is replaced by $N(\Lambda_b^0 \rightarrow J/\psi \Lambda) * \epsilon_{\text{rel}} * R_{\Xi_b^-/\Lambda_b^0}$. The simultaneous fit gives the same result as the weighted average for the ratio $R_{\Xi_b^-/\Lambda_b^0}$, and the mass difference is measured to be

$$\delta M = 177.08 \pm 0.47 \pm 0.16 \text{ MeV}/c^2.$$

This measurement is of similar precision to and consistent with the previous LHCb result $\delta M = 178.36 \pm 0.46 \pm 0.16 \text{ MeV}/c^2$ using

$\Xi_b^- \rightarrow \Xi_c^0 \pi^-$ and $\Lambda_b^0 \rightarrow \Lambda_c^+ \pi^-$ decays [11]. The two results are combined to obtain $\delta M = 177.73 \pm 0.33 \pm 0.14 \text{ MeV}/c^2$, where the correlations between the systematic uncertainties described below are properly taken into account.

Various sources of systematic uncertainty are considered for the mass difference measurement. The effect of the momentum scale uncertainty of 0.03% [32] leads to an uncertainty of $0.13 \text{ MeV}/c^2$. Because the signal mode has one more particle than the normalisation channel, the correction for energy loss in the detector material leads to an additional uncertainty of $0.06 \text{ MeV}/c^2$ [11,32]. The above two sources are fully correlated with the previous measurement using $\Xi_b^- \rightarrow \Xi_c^0 \pi^-$ and $\Lambda_b^0 \rightarrow \Lambda_c^+ \pi^-$ decays [11]. Uncertainties due to the signal and background modelling are 0.06 and $0.02 \text{ MeV}/c^2$, respectively, estimated by considering alternative functions as discussed in Sec. 6.

8. Conclusion

In conclusion, we report the first observation of the $\Xi_b^- \rightarrow J/\psi \Lambda K^-$ decay with a data sample of pp collisions corresponding to an integrated luminosity of 3 fb^{-1} . The observed signal yield is 308 ± 21 . In the kinematic region of the b -baryon transverse momentum $p_T < 25 \text{ GeV}/c$ and rapidity in the range $2.0 < y < 4.5$, the production rate of Ξ_b^- with $\Xi_b^- \rightarrow J/\psi \Lambda K^-$ decays relative to that of $\Lambda_b^0 \rightarrow J/\psi \Lambda$ decays is measured to be

$$\frac{f_{\Xi_b^-} \mathcal{B}(\Xi_b^- \rightarrow J/\psi \Lambda K^-)}{f_{\Lambda_b^0} \mathcal{B}(\Lambda_b^0 \rightarrow J/\psi \Lambda)} = (4.19 \pm 0.29 \text{ (stat)} \pm 0.15 \text{ (syst)}) \times 10^{-2},$$

where $f_{\Xi_b^-}/f_{\Lambda_b^0}$ is the ratio of the fragmentation fraction for $b \rightarrow \Xi_b^-$ and $b \rightarrow \Lambda_b^0$ transitions. The mass difference between Ξ_b^- and Λ_b^0 baryons is measured to be

$$M(\Xi_b^-) - M(\Lambda_b^0) = 177.08 \pm 0.47 \text{ (stat)} \pm 0.16 \text{ (syst)} \text{ MeV}/c^2.$$

A combination of this value with the previous LHCb measurement from $\Xi_b^- \rightarrow \Xi_c^0 \pi^-$ and $\Lambda_b^0 \rightarrow \Lambda_c^+ \pi^-$ decays [11] leads to the most precise value of the mass difference

$$M(\Xi_b^-) - M(\Lambda_b^0) = 177.73 \pm 0.33 \text{ (stat)} \pm 0.14 \text{ (syst)} \text{ MeV}/c^2.$$

With the full data sample accumulated before the long shutdown of the LHC in 2018, it should be possible to apply a full amplitude analysis to the $\Xi_b^- \rightarrow J/\psi \Lambda K^-$ decay to search for hidden-charm pentaquarks with open strangeness.

Acknowledgements

We express our gratitude to our colleagues in the CERN accelerator departments for the excellent performance of the LHC. We thank the technical and administrative staff at the LHCb institutes. We acknowledge support from CERN and from the national agencies: CAPES, CNPq, FAPERJ and FINEP (Brazil); NSFC (China); CNRS/IN2P3 (France); BMBF, DFG and MPG (Germany); INFN (Italy); FOM and NWO (The Netherlands); MNiSW and NCN (Poland); MEN/IFA (Romania); MinES and FASO (Russia); MINECO (Spain); SNSF and SER (Switzerland); NASU (Ukraine); STFC (United Kingdom); NSF (USA). We acknowledge the computing resources that are provided by CERN, IN2P3 (France), KIT and DESY (Germany), INFN (Italy), SURF (The Netherlands), PIC (Spain), GridPP (United Kingdom), RRCKI and Yandex LLC (Russia), CSCS (Switzerland), IFIN-HH (Romania), CBPF (Brazil), PL-GRID (Poland) and OSC

(USA). We are indebted to the communities behind the multiple open source software packages on which we depend. Individual groups or members have received support from AvH Foundation (Germany), EPLANET, Marie Skłodowska-Curie Actions and ERC (European Union), Conseil Général de Haute-Savoie, Labex ENIGMASS and OCEVU, Région Auvergne (France), RFBR and Yandex LLC (Russia), GVA, XuntaGal and GENCAT (Spain), Herchel Smith Fund, The Royal Society, Royal Commission for the Exhibition of 1851 and the Leverhulme Trust (United Kingdom).

References

- [1] M. Gell-Mann, A schematic model of baryons and mesons, *Phys. Lett.* 8 (1964) 214.
- [2] G. Zweig, An SU_3 model for strong interaction symmetry and its breaking, 1964, CERN-TH-401.
- [3] H.J. Lipkin, New possibilities for exotic hadrons – anticharmed strange baryons, *Phys. Lett. B* 195 (1987) 484.
- [4] LHCb collaboration, R. Aaij, et al., Observation of $J/\psi p$ resonances consistent with pentaquark states in $\Lambda_b^0 \rightarrow J/\psi p K^-$ decays, *Phys. Rev. Lett.* 115 (2015) 072001, arXiv:1507.03414.
- [5] LHCb collaboration, R. Aaij, et al., Study of the productions of Λ_b^0 and \bar{B}^0 hadrons in pp collisions and first measurement of the $\Lambda_b^0 \rightarrow J/\psi p K^-$ branching fraction, *Chin. Phys. C* 40 (2016) 011001, arXiv:1509.00292.
- [6] LHCb collaboration, R. Aaij, et al., Model-independent evidence for $J/\psi p$ contributions to $\Lambda_b^0 \rightarrow J/\psi p K^-$ decays, *Phys. Rev. Lett.* 117 (2016) 082002, arXiv:1604.05708.
- [7] H.-X. Chen, et al., Looking for a hidden-charm pentaquark state with strangeness $S = -1$ from Ξ_b^- decay into $J/\psi K^- \Lambda$, *Phys. Rev. C* 93 (2016) 065203, arXiv:1510.01803.
- [8] J.-J. Wu, R. Molina, E. Oset, B.S. Zou, Prediction of narrow N^* and Λ^* resonances with hidden charm above 4 GeV, *Phys. Rev. Lett.* 105 (2010) 232001, arXiv:1007.0573.
- [9] Particle Data Group, C. Patrignani, et al., Review of particle physics, *Chin. Phys. C* 40 (2016) 100001.
- [10] CDF collaboration, T. Aaltonen, et al., Mass and lifetime measurements of bottom and charm baryons in $p\bar{p}$ collisions at $\sqrt{s} = 1.96 \text{ TeV}$, *Phys. Rev. D* 89 (2014) 072014, arXiv:1403.8126.
- [11] LHCb collaboration, R. Aaij, et al., Precision measurement of the mass and lifetime of the Ψ_b^- baryon, *Phys. Rev. Lett.* 113 (2014) 242002, arXiv:1409.8568.
- [12] LHCb collaboration, A.A. Alves Jr., et al., The LHCb detector at the LHC, *J. Instrum.* 3 (2008) S08005.
- [13] LHCb collaboration, R. Aaij, et al., LHCb detector performance, *Int. J. Mod. Phys. A* 30 (2015) 1530022, arXiv:1412.6352.
- [14] R. Aaij, et al., The LHCb trigger and its performance in 2011, *J. Instrum.* 8 (2013) P04022, arXiv:1211.3055.
- [15] T. Sjöstrand, S. Mrenna, P. Skands, PYTHIA 6.4 physics and manual, *J. High Energy Phys.* 05 (2006) 026, arXiv:hep-ph/0603175.
- [16] T. Sjöstrand, S. Mrenna, P. Skands, A brief introduction to PYTHIA 8.1, *Comput. Phys. Commun.* 178 (2008) 852, arXiv:0710.3820.
- [17] I. Belyaev, et al., Handling of the generation of primary events in Gauss, the LHCb simulation framework, *J. Phys. Conf. Ser.* 331 (2011) 032047.
- [18] D.J. Lange, The EvtGen particle decay simulation package, *Nucl. Instrum. Methods A* 462 (2001) 152.
- [19] P. Golonka, Z. Was, PHOTOS Monte Carlo: a precision tool for QED corrections in Z and W decays, *Eur. Phys. J. C* 45 (2006) 97, arXiv:hep-ph/0506026.
- [20] Geant4 collaboration, J. Allison, et al., Geant4 developments and applications, *IEEE Trans. Nucl. Sci.* 53 (2006) 270.
- [21] Geant4 collaboration, S. Agostinelli, et al., Geant4: a simulation toolkit, *Nucl. Instrum. Methods A* 506 (2003) 250.
- [22] M. Clemencic, et al., The LHCb simulation application, Gauss: design, evolution and experience, *J. Phys. Conf. Ser.* 331 (2011) 032023.
- [23] L. Breiman, J.H. Friedman, R.A. Olshen, C.J. Stone, Classification and Regression Trees, Wadsworth International Group, Belmont, California, USA, 1984.
- [24] W.D. Hulsbergen, Decay chain fitting with a Kalman filter, *Nucl. Instrum. Methods A* 552 (2005) 566, arXiv:physics/0503191.
- [25] M. Adinolfi, et al., Performance of the LHCb RICH detector at the LHC, *Eur. Phys. J. C* 73 (2013) 2431, arXiv:1211.6759.
- [26] D. Martínez Santos, F. Dupertuis, Mass distributions marginalized over per-event errors, *Nucl. Instrum. Methods A* 764 (2014) 150, arXiv:1312.5000.
- [27] S.S. Wilks, The large-sample distribution of the likelihood ratio for testing composite hypotheses, *Ann. Math. Stat.* 9 (1938) 60.
- [28] M. Pivk, F.R. Le Diberder, sPlot: a statistical tool to unfold data distributions, *Nucl. Instrum. Methods A* 555 (2005) 356, arXiv:physics/0402083.

- [29] T. Skwarnicki, A Study of the Radiative Cascade Transitions Between the Upsilon-Prime and Upsilon Resonances, PhD thesis, Institute of Nuclear Physics, Krakow, 1986, DESY-F31-86-02.
- [30] LHCb collaboration, R. Aaij, et al., Measurement of the track reconstruction efficiency at LHCb, *J. Instrum.* 10 (2015) P02007, arXiv:1408.1251.
- [31] LHCb collaboration, R. Aaij, et al., Precision measurement of the ratio of the Λ_b^0 to B^0 lifetimes, *Phys. Lett. B* 734 (2014) 122, arXiv:1402.6242.
- [32] LHCb collaboration, R. Aaij, et al., Precision measurement of D meson mass differences, *J. High Energy Phys.* 06 (2013) 065, arXiv:1304.6865.

LHCb Collaboration

R. Aaij⁴⁰, B. Adeva³⁹, M. Adinolfi⁴⁸, Z. Ajaltouni⁵, S. Akar⁵⁹, J. Albrecht¹⁰, F. Alessio⁴⁰, M. Alexander⁵³, S. Ali⁴³, G. Alkhazov³¹, P. Alvarez Cartelle⁵⁵, A.A. Alves Jr⁵⁹, S. Amato², S. Amerio²³, Y. Amhis⁷, L. An³, L. Anderlini¹⁸, G. Andreassi⁴¹, M. Andreotti^{17,g}, J.E. Andrews⁶⁰, R.B. Appleby⁵⁶, F. Archilli⁴³, P. d'Argent¹², J. Arnau Romeu⁶, A. Artamonov³⁷, M. Artuso⁶¹, E. Aslanides⁶, G. Auriemma²⁶, M. Baalouch⁵, I. Babuschkin⁵⁶, S. Bachmann¹², J.J. Back⁵⁰, A. Badalov³⁸, C. Baesso⁶², S. Baker⁵⁵, V. Balagura^{7,c}, W. Baldini¹⁷, R.J. Barlow⁵⁶, C. Barschel⁴⁰, S. Barsuk⁷, W. Barter⁴⁰, F. Baryshnikov³², M. Baszczyk²⁷, V. Batozskaya²⁹, B. Batsukh⁶¹, V. Battista⁴¹, A. Bay⁴¹, L. Beaucourt⁴, J. Beddow⁵³, F. Bedeschi²⁴, I. Bediaga¹, L.J. Bel⁴³, V. Bellee⁴¹, N. Belloli^{21,i}, K. Belous³⁷, I. Belyaev³², E. Ben-Haim⁸, G. Bencivenni¹⁹, S. Benson⁴³, A. Berezhnoy³³, R. Bernet⁴², A. Bertolin²³, C. Betancourt⁴², F. Betti¹⁵, M.-O. Bettler⁴⁰, M. van Beuzekom⁴³, I.A. Bezshyiko⁴², S. Bifani⁴⁷, P. Billoir⁸, T. Bird⁵⁶, A. Birnkraut¹⁰, A. Bitadze⁵⁶, A. Bizzeti^{18,u}, T. Blake⁵⁰, F. Blanc⁴¹, J. Blouw^{11,†}, S. Blusk⁶¹, V. Bocci²⁶, T. Boettcher⁵⁸, A. Bondar^{36,w}, N. Bondar^{31,40}, W. Bonivento¹⁶, I. Bordyuzhin³², A. Borgheresi^{21,i}, S. Borghi⁵⁶, M. Borisyak³⁵, M. Borsato³⁹, F. Bossu⁷, M. Boubdir⁹, T.J.V. Bowcock⁵⁴, E. Bowen⁴², C. Bozzi^{17,40}, S. Braun¹², M. Britsch¹², T. Britton⁶¹, J. Brodzicka⁵⁶, E. Buchanan⁴⁸, C. Burr⁵⁶, A. Bursche², J. Buytaert⁴⁰, S. Cadeddu¹⁶, R. Calabrese^{17,g}, M. Calvi^{21,i}, M. Calvo Gomez^{38,m}, A. Camboni³⁸, P. Campana¹⁹, D.H. Campora Perez⁴⁰, L. Capriotti⁵⁶, A. Carbone^{15,e}, G. Carboni^{25,j}, R. Cardinale^{20,h}, A. Cardini¹⁶, P. Carniti^{21,i}, L. Carson⁵², K. Carvalho Akiba², G. Casse⁵⁴, L. Cassina^{21,i}, L. Castillo Garcia⁴¹, M. Cattaneo⁴⁰, G. Cavallero²⁰, R. Cenci^{24,t}, D. Chamont⁷, M. Charles⁸, Ph. Charpentier⁴⁰, G. Chatzikonstantinidis⁴⁷, M. Chefdeville⁴, S. Chen⁵⁶, S.-F. Cheung⁵⁷, V. Chobanova³⁹, M. Chruszcz^{42,27}, X. Cid Vidal³⁹, G. Ciezarek⁴³, P.E.L. Clarke⁵², M. Clemencic⁴⁰, H.V. Cliff⁴⁹, J. Closier⁴⁰, V. Coco⁵⁹, J. Cogan⁶, E. Cogneras⁵, V. Cogoni^{16,40,f}, L. Cojocariu³⁰, G. Collazuol^{23,o}, P. Collins⁴⁰, A. Comerma-Montells¹², A. Contu⁴⁰, A. Cook⁴⁸, G. Coombs⁴⁰, S. Coquereau³⁸, G. Corti⁴⁰, M. Corvo^{17,g}, C.M. Costa Sobral⁵⁰, B. Couturier⁴⁰, G.A. Cowan⁵², D.C. Craik⁵², A. Crocombe⁵⁰, M. Cruz Torres⁶², S. Cunliffe⁵⁵, R. Currie⁵⁵, C. D'Ambrosio⁴⁰, F. Da Cunha Marinho², E. Dall'Occo⁴³, J. Dalseno⁴⁸, P.N.Y. David⁴³, A. Davis³, K. De Bruyn⁶, S. De Capua⁵⁶, M. De Cian¹², J.M. De Miranda¹, L. De Paula², M. De Serio^{14,d}, P. De Simone¹⁹, C.T. Dean⁵³, D. Decamp⁴, M. Deckenhoff¹⁰, L. Del Buono⁸, M. Demmer¹⁰, A. Dendek²⁸, D. Derkach³⁵, O. Deschamps⁵, F. Dettori⁴⁰, B. Dey²², A. Di Canto⁴⁰, H. Dijkstra⁴⁰, F. Dordei⁴⁰, M. Dorigo⁴¹, A. Dosil Suárez³⁹, A. Dovbnya⁴⁵, K. Dreimanis⁵⁴, L. Dufour⁴³, G. Dujany⁵⁶, K. Dungs⁴⁰, P. Durante⁴⁰, R. Dzhelyadin³⁷, A. Dziurda⁴⁰, A. Dzyuba³¹, N. Déléage⁴, S. Easo⁵¹, M. Ebert⁵², U. Egede⁵⁵, V. Egorychev³², S. Eidelman^{36,w}, S. Eisenhardt⁵², U. Eitschberger¹⁰, R. Ekelhof¹⁰, L. Eklund⁵³, S. Ely⁶¹, S. Esen¹², H.M. Evans⁴⁹, T. Evans⁵⁷, A. Falabella¹⁵, N. Farley⁴⁷, S. Farry⁵⁴, R. Fay⁵⁴, D. Fazzini^{21,i}, D. Ferguson⁵², A. Fernandez Prieto³⁹, F. Ferrari^{15,40}, F. Ferreira Rodrigues², M. Ferro-Luzzi⁴⁰, S. Filippov³⁴, R.A. Fini¹⁴, M. Fiore^{17,g}, M. Fiorini^{17,g}, M. Firlej²⁸, C. Fitzpatrick⁴¹, T. Fiutowski²⁸, F. Fleuret^{7,b}, K. Fohl⁴⁰, M. Fontana^{16,40}, F. Fontanelli^{20,h}, D.C. Forshaw⁶¹, R. Forty⁴⁰, V. Franco Lima⁵⁴, M. Frank⁴⁰, C. Frei⁴⁰, J. Fu^{22,q}, W. Funk⁴⁰, E. Furfaro^{25,j}, C. Färber⁴⁰, A. Gallas Torreira³⁹, D. Galli^{15,e}, S. Gallorini²³, S. Gambetta⁵², M. Gandelman², P. Gandini⁵⁷, Y. Gao³, L.M. Garcia Martin⁶⁹, J. García Pardiñas³⁹, J. Garra Tico⁴⁹, L. Garrido³⁸, P.J. Garsed⁴⁹, D. Gascon³⁸, C. Gaspar⁴⁰, L. Gavardi¹⁰, G. Gazzoni⁵, D. Gerick¹², E. Gersabeck¹², M. Gersabeck⁵⁶, T. Gershon⁵⁰, Ph. Ghez⁴, S. Gianì⁴¹, V. Gibson⁴⁹, O.G. Girard⁴¹, L. Giubega³⁰, K. Gizdov⁵², V.V. Gligorov⁸, D. Golubkov³², A. Golutvin^{55,40}, A. Gomes^{1,a}, I.V. Gorelov³³, C. Gotti^{21,i}, R. Graciani Diaz³⁸, L.A. Granado Cardoso⁴⁰, E. Graugés³⁸, E. Graverini⁴², G. Graziani¹⁸, A. Greco³⁰, P. Griffith⁴⁷, L. Grillo^{21,40,i}, B.R. Gruberg Cazon⁵⁷, O. Grünberg⁶⁷, E. Gushchin³⁴, Yu. Guz³⁷, T. Gys⁴⁰, C. Göbel⁶², T. Hadavizadeh⁵⁷, C. Hadjivasiliou⁵, G. Haefeli⁴¹, C. Haen⁴⁰, S.C. Haines⁴⁹, B. Hamilton⁶⁰, X. Han¹², S. Hansmann-Menzemer¹², N. Harnew⁵⁷, S.T. Harnew⁴⁸, J. Harrison⁵⁶, M. Hatch⁴⁰, J. He⁶³, T. Head⁴¹, A. Heister⁹, K. Hennessy⁵⁴, P. Henrard⁵, L. Henry⁸, E. van Herwijnen⁴⁰, M. Heß⁶⁷, A. Hicheur², D. Hill⁵⁷, C. Hombach⁵⁶,

H. Hopchev⁴¹, W. Hulsbergen⁴³, T. Humair⁵⁵, M. Hushchyn³⁵, D. Hutchcroft⁵⁴, M. Idzik²⁸, P. Ilten⁵⁸, R. Jacobsson⁴⁰, A. Jaeger¹², J. Jalocho⁵⁷, E. Jans⁴³, A. Jawahery⁶⁰, F. Jiang³, M. John⁵⁷, D. Johnson⁴⁰, C.R. Jones⁴⁹, C. Joram⁴⁰, B. Jost⁴⁰, N. Jurik⁵⁷, S. Kandybei⁴⁵, M. Karacson⁴⁰, J.M. Kariuki⁴⁸, S. Karodia⁵³, M. Kecke¹², M. Kelsey⁶¹, M. Kenzie⁴⁹, T. Ketel⁴⁴, E. Khairullin³⁵, B. Khanji¹², C. Khurewathanakul⁴¹, T. Kirn⁹, S. Klaver⁵⁶, K. Klimaszewski²⁹, S. Koliiiev⁴⁶, M. Kolpin¹², I. Komarov⁴¹, R.F. Koopman⁴⁴, P. Koppenburg⁴³, A. Kosmyntseva³², A. Kozachuk³³, M. Kozeiha⁵, L. Kravchuk³⁴, K. Kreplin¹², M. Kreps⁵⁰, P. Krokovny^{36,w}, F. Kruse¹⁰, W. Krzemien²⁹, W. Kucewicz^{27,l}, M. Kucharczyk²⁷, V. Kudryavtsev^{36,w}, A.K. Kuonen⁴¹, K. Kurek²⁹, T. Kvaratskheliya^{32,40}, D. Lacarrere⁴⁰, G. Lafferty⁵⁶, A. Lai¹⁶, G. Lanfranchi¹⁹, C. Langenbruch⁹, T. Latham⁵⁰, C. Lazzeroni⁴⁷, R. Le Gac⁶, J. van Leerdam⁴³, A. Leflat^{33,40}, J. Lefrançois⁷, R. Lefèvre⁵, F. Lemaitre⁴⁰, E. Lemos Cid³⁹, O. Leroy⁶, T. Lesiak²⁷, B. Leverington¹², T. Li³, Y. Li⁷, T. Likhomanenko^{35,68}, R. Lindner⁴⁰, C. Linn⁴⁰, F. Lionetto⁴², X. Liu^{3,*}, D. Loh⁵⁰, I. Longstaff⁵³, J.H. Lopes², D. Lucchesi^{23,o}, M. Lucio Martinez³⁹, H. Luo⁵², A. Lupato²³, E. Luppi^{17,g}, O. Lupton⁴⁰, A. Lusiani²⁴, X. Lyu⁶³, F. Machefert⁷, F. Maciuc³⁰, O. Maev³¹, K. Maguire⁵⁶, S. Malde⁵⁷, A. Malinin⁶⁸, T. Maltsev³⁶, G. Manca^{16,f}, G. Mancinelli⁶, P. Manning⁶¹, J. Maratas^{5,v}, J.F. Marchand⁴, U. Marconi¹⁵, C. Marin Benito³⁸, M. Marinangeli⁴¹, P. Marino^{24,t}, J. Marks¹², G. Martellotti²⁶, M. Martin⁶, M. Martinelli⁴¹, D. Martinez Santos³⁹, F. Martinez Vidal⁶⁹, D. Martins Tostes², L.M. Massacrier⁷, A. Massafferri¹, R. Matev⁴⁰, A. Mathad⁵⁰, Z. Mathe⁴⁰, C. Matteuzzi²¹, A. Mauri⁴², E. Maurice^{7,b}, B. Maurin⁴¹, A. Mazurov⁴⁷, M. McCann^{55,40}, A. McNab⁵⁶, R. McNulty¹³, B. Meadows⁵⁹, F. Meier¹⁰, M. Meissner¹², D. Melnychuk²⁹, M. Merk⁴³, A. Merli^{22,q}, E. Michielin²³, D.A. Milanes⁶⁶, M.-N. Minard⁴, D.S. Mitzel¹², A. Mogini⁸, J. Molina Rodriguez¹, I.A. Monroy⁶⁶, S. Monteil⁵, M. Morandin²³, P. Morawski²⁸, A. Mordà⁶, M.J. Morello^{24,t}, O. Morgunova⁶⁸, J. Moron²⁸, A.B. Morris⁵², R. Mountain⁶¹, F. Muheim⁵², M. Mulder⁴³, M. Mussini¹⁵, D. Müller⁵⁶, J. Müller¹⁰, K. Müller⁴², V. Müller¹⁰, P. Naik⁴⁸, T. Nakada⁴¹, R. Nandakumar⁵¹, A. Nandi⁵⁷, I. Nasteva², M. Needham⁵², N. Neri²², S. Neubert¹², N. Neufeld⁴⁰, M. Neuner¹², T.D. Nguyen⁴¹, C. Nguyen-Mau^{41,n}, S. Nieswand⁹, R. Niet¹⁰, N. Nikitin³³, T. Nikodem¹², A. Nogay⁶⁸, A. Novoselov³⁷, D.P. O'Hanlon⁵⁰, A. Oblakowska-Mucha²⁸, V. Obraztsov³⁷, S. Ogilvy¹⁹, R. Oldeman^{16,f}, C.J.G. Onderwater⁷⁰, J.M. Otalora Goicochea², A. Otto⁴⁰, P. Owen⁴², A. Oyanguren⁶⁹, P.R. Pais⁴¹, A. Palano^{14,d}, F. Palombo^{22,q}, M. Palutan¹⁹, A. Papanestis⁵¹, M. Pappagallo^{14,d}, L.L. Pappalardo^{17,g}, W. Parker⁶⁰, C. Parkes⁵⁶, G. Passaleva¹⁸, A. Pastore^{14,d}, G.D. Patel⁵⁴, M. Patel⁵⁵, C. Patrignani^{15,e}, A. Pearce⁴⁰, A. Pellegrino⁴³, G. Penso²⁶, M. Pepe Altarelli⁴⁰, S. Perazzini⁴⁰, P. Perret⁵, L. Pescatore⁴⁷, K. Petridis⁴⁸, A. Petrolini^{20,h}, A. Petrov⁶⁸, M. Petruzzo^{22,q}, E. Picatoste Olloqui³⁸, B. Pietrzyk⁴, M. Pikies²⁷, D. Pinci²⁶, A. Pistone²⁰, A. Piucci¹², V. Placinta³⁰, S. Playfer⁵², M. Plo Casasus³⁹, T. Poikela⁴⁰, F. Polci⁸, A. Poluektov^{50,36}, I. Polyakov⁶¹, E. Polcarpo², G.J. Pomery⁴⁸, A. Popov³⁷, D. Popov^{11,40}, B. Popovici³⁰, S. Poslavskii³⁷, C. Potterat², E. Price⁴⁸, J.D. Price⁵⁴, J. Prisciandaro^{39,40}, A. Pritchard⁵⁴, C. Prouve⁴⁸, V. Pugatch⁴⁶, A. Puig Navarro⁴², G. Punzi^{24,p}, W. Qian⁵⁰, R. Quagliani^{7,48}, B. Rachwal²⁷, J.H. Rademacker⁴⁸, M. Rama²⁴, M. Ramos Pernas³⁹, M.S. Rangel², I. Raniuk⁴⁵, F. Ratnikov³⁵, G. Raven⁴⁴, F. Redi⁵⁵, S. Reichert¹⁰, A.C. dos Reis¹, C. Remon Alepuz⁶⁹, V. Renaudin⁷, S. Ricciardi⁵¹, S. Richards⁴⁸, M. Rihl⁴⁰, K. Rinnert⁵⁴, V. Rives Molina³⁸, P. Robbe^{7,40}, A.B. Rodrigues¹, E. Rodrigues⁵⁹, J.A. Rodriguez Lopez⁶⁶, P. Rodriguez Perez^{56,†}, A. Rogozhnikov³⁵, S. Roiser⁴⁰, A. Rollings⁵⁷, V. Romanovskiy³⁷, A. Romero Vidal³⁹, J.W. Ronayne¹³, M. Rotondo¹⁹, M.S. Rudolph⁶¹, T. Ruf⁴⁰, P. Ruiz Valls⁶⁹, J.J. Saborido Silva³⁹, E. Sadykhov³², N. Sagidova³¹, B. Saitta^{16,f}, V. Salustino Guimaraes¹, C. Sanchez Mayordomo⁶⁹, B. Sanmartin Sedes³⁹, R. Santacesaria²⁶, C. Santamarina Rios³⁹, M. Santimaria¹⁹, E. Santovetti^{25,j}, A. Sarti^{19,k}, C. Satriano^{26,s}, A. Satta²⁵, D.M. Saunders⁴⁸, D. Savrina^{32,33}, S. Schael⁹, M. Schellenberg¹⁰, M. Schiller⁵³, H. Schindler⁴⁰, M. Schlupp¹⁰, M. Schmelling¹¹, T. Schmelzer¹⁰, B. Schmidt⁴⁰, O. Schneider⁴¹, A. Schopper⁴⁰, K. Schubert¹⁰, M. Schubiger⁴¹, M.-H. Schune⁷, R. Schwemmer⁴⁰, B. Sciascia¹⁹, A. Sciubba^{26,k}, A. Semennikov³², A. Sergi⁴⁷, N. Serra⁴², J. Serrano⁶, L. Sestini²³, P. Seyfert²¹, M. Shapkin³⁷, I. Shapoval⁴⁵, Y. Shcheglov³¹, T. Shears⁵⁴, L. Shekhtman^{36,w}, V. Shevchenko⁶⁸, B.G. Siddi^{17,40}, R. Silva Coutinho⁴², L. Silva de Oliveira², G. Simi^{23,o}, S. Simone^{14,d}, M. Sirendi⁴⁹, N. Skidmore⁴⁸, T. Skwarnicki⁶¹, E. Smith⁵⁵, I.T. Smith⁵², J. Smith⁴⁹, M. Smith⁵⁵, H. Snoek⁴³, L. Soares Lavra¹, M.D. Sokoloff⁵⁹, F.J.P. Soler⁵³, B. Souza De Paula², B. Spaan¹⁰, P. Spradlin⁵³, S. Sridharan⁴⁰, F. Stagni⁴⁰, M. Stahl¹², S. Stahl⁴⁰, P. Stefko⁴¹, S. Stefkova⁵⁵, O. Steinkamp⁴², S. Stemmler¹², O. Stenyakin³⁷,

H. Stevens¹⁰, S. Stevenson⁵⁷, S. Stoica³⁰, S. Stone⁶¹, B. Storaci⁴², S. Stracka^{24,p}, M. Straticiu³⁰, U. Straumann⁴², L. Sun⁶⁴, W. Sutcliffe⁵⁵, K. Swientek²⁸, V. Syropoulos⁴⁴, M. Szczekowski²⁹, T. Szumlak²⁸, S. T'Jampens⁴, A. Tayduganov⁶, T. Tekampe¹⁰, G. Tellarini^{17,g}, F. Teubert⁴⁰, E. Thomas⁴⁰, J. van Tilburg⁴³, M.J. Tilley⁵⁵, V. Tisserand⁴, M. Tobin⁴¹, S. Tolk⁴⁹, L. Tomassetti^{17,g}, D. Tonelli⁴⁰, S. Topp-Joergensen⁵⁷, F. Toriello⁶¹, E. Tournefier⁴, S. Tourneur⁴¹, K. Trabelsi⁴¹, M. Traill⁵³, M.T. Tran⁴¹, M. Tresch⁴², A. Trisovic⁴⁰, A. Tsaregorodtsev⁶, P. Tsopelas⁴³, A. Tully⁴⁹, N. Tuning⁴³, A. Ukleja²⁹, A. Ustyuzhanin³⁵, U. Uwer¹², C. Vacca^{16,f}, V. Vagnoni^{15,40}, A. Valassi⁴⁰, S. Valat⁴⁰, G. Valenti¹⁵, R. Vazquez Gomez¹⁹, P. Vazquez Regueiro³⁹, S. Vecchi¹⁷, M. van Veghel⁴³, J.J. Velthuis⁴⁸, M. Veltri^{18,r}, G. Veneziano⁵⁷, A. Venkateswaran⁶¹, M. Vernet⁵, M. Vesterinen¹², J.V. Viana Barbosa⁴⁰, B. Viaud⁷, D. Vieira⁶³, M. Vieites Diaz³⁹, H. Viemann⁶⁷, X. Vilasis-Cardona^{38,m}, M. Vitti⁴⁹, V. Volkov³³, A. Vollhardt⁴², B. Voneki⁴⁰, A. Vorobyev³¹, V. Vorobyev^{36,w}, C. Voß⁹, J.A. de Vries⁴³, C. Vázquez Sierra³⁹, R. Waldi⁶⁷, C. Wallace⁵⁰, R. Wallace¹³, J. Walsh²⁴, J. Wang⁶¹, D.R. Ward⁴⁹, H.M. Wark⁵⁴, N.K. Watson⁴⁷, D. Websdale⁵⁵, A. Weiden⁴², M. Whitehead⁴⁰, J. Wicht⁵⁰, G. Wilkinson^{57,40}, M. Wilkinson⁶¹, M. Williams⁴⁰, M.P. Williams⁴⁷, M. Williams⁵⁸, T. Williams⁴⁷, F.F. Wilson⁵¹, J. Wimberley⁶⁰, J. Wishahi¹⁰, W. Wislicki²⁹, M. Witek²⁷, G. Wormser⁷, S.A. Wotton⁴⁹, K. Wraight⁵³, K. Wyllie⁴⁰, Y. Xie⁶⁵, Z. Xing⁶¹, Z. Xu⁴¹, Z. Yang³, Y. Yao⁶¹, H. Yin⁶⁵, J. Yu⁶⁵, X. Yuan^{36,w}, O. Yushchenko³⁷, K.A. Zarebski⁴⁷, M. Zavertyaev^{11,c}, L. Zhang³, Y. Zhang⁷, Y. Zhang⁶³, A. Zhelezov¹², Y. Zheng⁶³, X. Zhu³, V. Zhukov³³, S. Zucchelli¹⁵

¹ Centro Brasileiro de Pesquisas Físicas (CBPF), Rio de Janeiro, Brazil

² Universidade Federal do Rio de Janeiro (UFRJ), Rio de Janeiro, Brazil

³ Center for High Energy Physics, Tsinghua University, Beijing, China

⁴ LAPP, Université Savoie Mont-Blanc, CNRS/IN2P3, Annecy-Le-Vieux, France

⁵ Clermont Université, Université Blaise Pascal, CNRS/IN2P3, LPC, Clermont-Ferrand, France

⁶ CPPM, Aix-Marseille Université, CNRS/IN2P3, Marseille, France

⁷ LAL, Université Paris-Sud, CNRS/IN2P3, Orsay, France

⁸ LPNHE, Université Pierre et Marie Curie, Université Paris Diderot, CNRS/IN2P3, Paris, France

⁹ I. Physikalisches Institut, RWTH Aachen University, Aachen, Germany

¹⁰ Fakultät Physik, Technische Universität Dortmund, Dortmund, Germany

¹¹ Max-Planck-Institut für Kernphysik (MPIK), Heidelberg, Germany

¹² Physikalisches Institut, Ruprecht-Karls-Universität Heidelberg, Heidelberg, Germany

¹³ School of Physics, University College Dublin, Dublin, Ireland

¹⁴ Sezione INFN di Bari, Bari, Italy

¹⁵ Sezione INFN di Bologna, Bologna, Italy

¹⁶ Sezione INFN di Cagliari, Cagliari, Italy

¹⁷ Sezione INFN di Ferrara, Ferrara, Italy

¹⁸ Sezione INFN di Firenze, Firenze, Italy

¹⁹ Laboratori Nazionali dell'INFN di Frascati, Frascati, Italy

²⁰ Sezione INFN di Genova, Genova, Italy

²¹ Sezione INFN di Milano Bicocca, Milano, Italy

²² Sezione INFN di Milano, Milano, Italy

²³ Sezione INFN di Padova, Padova, Italy

²⁴ Sezione INFN di Pisa, Pisa, Italy

²⁵ Sezione INFN di Roma Tor Vergata, Roma, Italy

²⁶ Sezione INFN di Roma La Sapienza, Roma, Italy

²⁷ Henryk Niewodniczanski Institute of Nuclear Physics Polish Academy of Sciences, Kraków, Poland

²⁸ AGH – University of Science and Technology, Faculty of Physics and Applied Computer Science, Kraków, Poland

²⁹ National Center for Nuclear Research (NCBJ), Warsaw, Poland

³⁰ Horia Hulubei National Institute of Physics and Nuclear Engineering, Bucharest-Magurele, Romania

³¹ Petersburg Nuclear Physics Institute (PNPI), Gatchina, Russia

³² Institute of Theoretical and Experimental Physics (ITEP), Moscow, Russia

³³ Institute of Nuclear Physics, Moscow State University (SINP MSU), Moscow, Russia

³⁴ Institute for Nuclear Research of the Russian Academy of Sciences (INR RAN), Moscow, Russia

³⁵ Yandex School of Data Analysis, Moscow, Russia

³⁶ Budker Institute of Nuclear Physics (SB RAS), Novosibirsk, Russia

³⁷ Institute for High Energy Physics (IHEP), Protvino, Russia

³⁸ ICCUB, Universitat de Barcelona, Barcelona, Spain

³⁹ Universidad de Santiago de Compostela, Santiago de Compostela, Spain

⁴⁰ European Organization for Nuclear Research (CERN), Geneva, Switzerland

⁴¹ Institute of Physics, Ecole Polytechnique Fédérale de Lausanne (EPFL), Lausanne, Switzerland

⁴² Physik-Institut, Universität Zürich, Zürich, Switzerland

⁴³ Nikhef National Institute for Subatomic Physics, Amsterdam, The Netherlands

⁴⁴ Nikhef National Institute for Subatomic Physics and VU University Amsterdam, Amsterdam, The Netherlands

⁴⁵ NSC Kharkiv Institute of Physics and Technology (NSC KIPT), Kharkiv, Ukraine

⁴⁶ Institute for Nuclear Research of the National Academy of Sciences (KINR), Kyiv, Ukraine

⁴⁷ University of Birmingham, Birmingham, United Kingdom

⁴⁸ H.H. Wills Physics Laboratory, University of Bristol, Bristol, United Kingdom

⁴⁹ Cavendish Laboratory, University of Cambridge, Cambridge, United Kingdom

⁵⁰ Department of Physics, University of Warwick, Coventry, United Kingdom

⁵¹ STFC Rutherford Appleton Laboratory, Didcot, United Kingdom

- ⁵² School of Physics and Astronomy, University of Edinburgh, Edinburgh, United Kingdom
⁵³ School of Physics and Astronomy, University of Glasgow, Glasgow, United Kingdom
⁵⁴ Oliver Lodge Laboratory, University of Liverpool, Liverpool, United Kingdom
⁵⁵ Imperial College London, London, United Kingdom
⁵⁶ School of Physics and Astronomy, University of Manchester, Manchester, United Kingdom
⁵⁷ Department of Physics, University of Oxford, Oxford, United Kingdom
⁵⁸ Massachusetts Institute of Technology, Cambridge, MA, United States
⁵⁹ University of Cincinnati, Cincinnati, OH, United States
⁶⁰ University of Maryland, College Park, MD, United States
⁶¹ Syracuse University, Syracuse, NY, United States
⁶² Pontifícia Universidade Católica do Rio de Janeiro (PUC-Rio), Rio de Janeiro, Brazil ^x
⁶³ University of Chinese Academy of Sciences, Beijing, China ^y
⁶⁴ School of Physics and Technology, Wuhan University, Wuhan, China ^y
⁶⁵ Institute of Particle Physics, Central China Normal University, Wuhan, Hubei, China ^y
⁶⁶ Departamento de Física, Universidad Nacional de Colombia, Bogotá, Colombia ^z
⁶⁷ Institut für Physik, Universität Rostock, Rostock, Germany ^{aa}
⁶⁸ National Research Centre Kurchatov Institute, Moscow, Russia ^{ab}
⁶⁹ Instituto de Física Corpuscular, Centro Mixto Universidad de Valencia – CSIC, Valencia, Spain ^{ac}
⁷⁰ Van Swinderen Institute, University of Groningen, Groningen, The Netherlands ^{ad}

* Corresponding author.

E-mail address: xuesong.liu@cern.ch (X. Liu).

^a Universidade Federal do Triângulo Mineiro (UFTM), Uberaba-MG, Brazil.

^b Laboratoire Leprince-Ringuet, Palaiseau, France.

^c P.N. Lebedev Physical Institute, Russian Academy of Science (LPI RAS), Moscow, Russia.

^d Università di Bari, Bari, Italy.

^e Università di Bologna, Bologna, Italy.

^f Università di Cagliari, Cagliari, Italy.

^g Università di Ferrara, Ferrara, Italy.

^h Università di Genova, Genova, Italy.

ⁱ Università di Milano Bicocca, Milano, Italy.

^j Università di Roma Tor Vergata, Roma, Italy.

^k Università di Roma La Sapienza, Roma, Italy.

^l AGH – University of Science and Technology, Faculty of Computer Science, Electronics and Telecommunications, Kraków, Poland.

^m LIFAELS, La Salle, Universitat Ramon Llull, Barcelona, Spain.

ⁿ Hanoi University of Science, Hanoi, Viet Nam.

^o Università di Padova, Padova, Italy.

^p Università di Pisa, Pisa, Italy.

^q Università degli Studi di Milano, Milano, Italy.

^r Università di Urbino, Urbino, Italy.

^s Università della Basilicata, Potenza, Italy.

^t Scuola Normale Superiore, Pisa, Italy.

^u Università di Modena e Reggio Emilia, Modena, Italy.

^v Iligan Institute of Technology (IIT), Iligan, Philippines.

^w Novosibirsk State University, Novosibirsk, Russia.

^x Associated to Universidade Federal do Rio de Janeiro (UFRJ), Rio de Janeiro, Brazil.

^y Associated to Center for High Energy Physics, Tsinghua University, Beijing, China.

^z Associated to LPNHE, Université Pierre et Marie Curie, Université Paris Diderot, CNRS/IN2P3, Paris, France.

^{aa} Associated to Physikalisches Institut, Ruprecht-Karls-Universität Heidelberg, Heidelberg, Germany.

^{ab} Associated to Institute of Theoretical and Experimental Physics (ITEP), Moscow, Russia.

^{ac} Associated to ICCUB, Universitat de Barcelona, Barcelona, Spain.

^{ad} Associated to Nikhef National Institute for Subatomic Physics, Amsterdam, The Netherlands.

† Deceased.